Pol. J. Environ. Stud. Vol. XX, No. X (XXXX), 1-16
DOI: *10.15244/pjoes/209840* ONLINE PUBLICATION DATE: 2025-10-02

Original Research

Design and Valuation of Rainfall Derivatives within the Yangtze River Economic Belt in China

Yi Li°*, Bing Zhou

Institute for Chengdu-Chongqing Economic Zone Development, Chongqing Technology and Business University, Chongqing 400067, China

Received: 1 July 2025
Accepted: 23 August 2025

Abstract

In the Yangtze River Economic Belt, extreme rainfall events have a substantial impact on economic activities in agriculture, energy consumption, and associated industries. Consequently, precise rainfall forecasting is of paramount importance for these sectors. This study utilizes rainfall data from 11 provinces (municipalities) within the Yangtze River Economic Belt spanning from 2004 to 2023 to construct both the Seasonal Autoregressive Integrated Moving Average (SARIMA) model and the Ornstein-Uhlenbeck (O-U) model for the rainfall index. Based on the models' fitting performance, a more appropriate rainfall index prediction model is selected. Furthermore, by integrating option pricing theory, this paper designs an option contract contingent on rainfall. Through the analysis of rainfall prediction in the Yangtze River Economic Belt and its derivative pricing, we have identified several key findings. Firstly, after differential processing, the rainfall data from this region exhibits stability, making it suitable for time series model analysis. Secondly, by fitting the rainfall data using both the SARIMA and O-U models, we found that the predicted values closely align with actual observations, indicating that these models provide accurate fits. Thirdly, employing the SARIMA and O-U models simulation to predict rainfall, we observed that the SARIMA model yields superior fit accuracy when comparing their respective errors. Fourthly, option contracts designed based on the SARIMA model reveal that increased climate volatility and higher climate risk correlate with higher pricing. Additionally, this study explores the practical application potential of weather derivatives in the Yangtze River Economic Belt and how they can be utilized to mitigate climate risks associated with rainfall fluctuations. The overarching goal is to effectively reduce climate risks faced by industries within the Yangtze River Economic Belt through scientifically sound rainfall predictions and derivative pricing, thereby promoting regional economic stability.

Keywords: climate risk, SARIMA model, option pricing model, rainfall prediction, weather derivatives pricing

*e-mail: liyi21@ctbu.edu.cn
°ORCID iD: 0009-0002-6611-9736

Introduction

Since the Industrial Revolution, global temperatures have risen by about 1.1ºC, and this trend is expected to continue [1]. This will lead to an increase in extreme climate events, such as extreme rainfall. The Yangtze River Economic Belt, one of China's most economically active regions, is vulnerable to natural disasters such as floods and mudslides caused by extreme rainfall. According to the "China Flood and Drought Disaster Bulletin" (2016-2020), the annual direct economic losses from flooding in the 11 provinces and municipalities within this region amounted to 135.4 billion yuan, accounting for 54% of the national total during that period. Over 230 million people were affected, representing 62.6% of the national total. More than 4.5 million hectares of farmland were damaged annually, constituting 51% of the country's total affected area [2]. Therefore, analyzing precipitation patterns in the Yangtze River Economic Belt is crucial to enhancing climate risk prevention capabilities and providing scientific support for soil and water conservation efforts.

In recent years, weather derivatives - financial instruments based on meteorological indices - have gained increasing attention in addressing disaster risks caused by climate change. Compared to traditional agricultural insurance, these derivatives offer several advantages. Traditional agricultural insurance typically bases claims on crop yields or income. This makes it susceptible to moral hazards and adverse selection. The claim processes are cumbersome, and the responses are delayed [3]. However, weather index insurance products rely on objective meteorological data, effectively avoiding moral hazards stemming from information asymmetry. Additionally, weather derivatives' streamlined claims process eliminates the need for on-site loss assessments, significantly improving compensation efficiency and providing farmers and businesses with timely risk protection. International experience also demonstrates that weather derivatives excel at mitigating the economic impacts of extreme weather events. For example, countries such as Switzerland and the United States have substantially increased the resilience of their agriculture and energy sectors through weather options [4]. In China, as related products gain wider adoption and policy support strengthens, weather derivatives are poised to become a crucial supplementary tool for regional climate risk management.

Scholars worldwide have laid the groundwork for weather derivatives research. The relevant literature primarily focuses on two aspects: weather prediction models and financial instruments in climate risk management. First, various methods have been proposed for weather forecasting: the O-U model [5, 6], time series models [7], and machine learning algorithms [8]. Second, financial instruments for climate risk management mainly include traditional agricultural insurance [9] and weather derivatives [10]. Traditional agriculture insurance, plagued by high claims costs, information asymmetry, and lengthy claim processing times, has driven the emergence of weather derivatives. As a financial risk transfer tool, weather derivatives offer advantages such as flexibility, operational simplicity, and high marketization [11]. However, their limitations include limited market scale, a lack of mature pricing models, inadequate regulatory mechanisms, and restricted adoption due to policy and technological constraints.

In conclusion, weather derivatives demonstrate unique advantages. However, research on this subject is limited, especially regarding rainfall analysis in the Yangtze River Economic Belt, where existing studies are insufficient. This study aims to provide new perspectives and practical tools for climate risk management and promote sustainable economic development by conducting an in-depth analysis of rainfall forecasting and derivative pricing within the Yangtze River Economic Belt.

Compared with existing studies, this paper's innovations are reflected in three aspects. First, it focuses on the Yangtze River Economic Belt to enhance regional characteristic analysis. Second, it employs multiple models for rainfall prediction, demonstrating greater scientific validity and rationality than single models. Third, it innovatively designs practical rainfall derivatives tailored to real-world needs. These derivatives provide more effective risk transfer channels for local governments and enterprises, thereby promoting the in-depth development of climate risk financialization.

The remainder of this paper is organized as follows: the second part elaborates on the theoretical framework underlying this study. The third part uses the SARIMA model to forecast rainfall, and the fourth part uses the O-U model for similar predictions. The fifth part prices weather derivatives by integrating the forecast results with an option pricing model. The sixth part examines the practical applications of weather derivatives. Finally, the seventh part summarizes the key findings, the limitations of this paper, and the future research direction.

Materials and Methods

The Prediction Model of the Climate Index

SARIMA

The concept of time series primarily denotes that a random variable evolves in response to temporal changes, exhibiting autocorrelation, which suggests a degree of continuity in the predicted variable. This characteristic allows for the development of mathematical models that can express this relationship, thereby enabling predictions of future trends based on historical data [12]. The Seasonal Autoregressive

Integrated Moving Average (SARIMA) model extends this foundation by accounting for periodic patterns within the time series. To enhance the prediction accuracy for non-stationary time series, SARIMA builds upon the ARIMA framework, incorporating seasonal components. The ARIMA model, or Autoregressive Integrated Moving Average model, is extensively utilized in academia. It achieves stationarity through differencing and subsequently performs predictive analysis on the transformed data [13]. According to relevant literature [14], the general form of the ARIMA model is as follows:

$$\Phi(\mathrm{B})(1-\mathrm{B})^{d}\,\mathrm{x_t} = \theta(B)\varepsilon_t \tag{1}$$

The aforementioned equation represents the ARIMA(p,d,q) model. In this context, x_t denotes the time series data, ε_t signifies a zero-mean white noise sequence, p indicates the autoregressive order, q denotes the moving average order, and d represents the differencing order. B is the lag operator, Φ(B) is the polynomial of autoregressive coefficients, and θ(B) is the polynomial of moving average coefficients. Typically, this model is more appropriate when the selected sequence exhibits significant time trends or seasonal variations. According to relevant literature [15], the general form of the SARIMA model is as follows:

$$\Phi(\mathrm{B})\Phi(\mathrm{B^s})(1-\mathrm{B})^{\mathrm{D}}\,\mathrm{x_t} = \mathrm{c} + \theta(\mathrm{B})\Theta(\mathrm{B^s})\varepsilon_{\mathrm{t}} \tag{2}$$

The formula represents the SARIMA(p,d,q)$(P,D,Q)_s$ model. Here, B^s denotes the length of the seasonal cycle, D represents the order of seasonal differencing, B_s is the seasonal backshift operator, while P and Q denote the orders of the seasonal autoregressive and seasonal moving average components, respectively.

$$\mathrm{x_{t\text{-}p}} = B^{p}x_t \tag{3}$$

If the difference operation is expressed by the delay operator, the d-th order difference can be expressed as:

$$\nabla^{\mathrm{d}}\mathrm{x_t} = (1-\mathrm{B})^{\mathrm{d}}\mathrm{x_t} \tag{4}$$

And the polynomials related to B in the formula can be expressed respectively as:

$$\Phi\ (\mathrm{B}) = 1-\Phi_1\mathrm{B}-\Phi_2\mathrm{B}^2\ldots-\Phi_p\mathrm{B}^{\mathrm{p}} \tag{5}$$

$$\theta\ (\mathrm{B}) = 1-\theta_1\mathrm{B}-\theta_2\mathrm{B}^2\ldots-\theta_{\mathrm{q}}\mathrm{B}^{\mathrm{q}} \tag{6}$$

$$\Phi_{\mathrm{s}}(\mathrm{B}) = 1-\Phi_1\mathrm{B}^{\mathrm{s}}-\Phi_2\mathrm{B}^{2\mathrm{S}}\ldots-\Phi_p\mathrm{B}^{\mathrm{PS}} \tag{7}$$

$$\Theta_{\mathrm{s}}(\mathrm{B}) = 1-\Theta_1\mathrm{B}^{\mathrm{S}}-\Theta_2\mathrm{B}^{2\mathrm{S}}\ldots-\Theta_{\mathrm{Q}}\mathrm{B}^{\mathrm{QS}} \tag{8}$$

O-U

Typically, following the application of differencing procedures, the corresponding climate index tends to exhibit characteristics consistent with a normal distribution and demonstrates pronounced mean-reverting properties. Consequently, in alignment with relevant literature [16], the Ornstein-Uhlenbeck (O-U) model is employed for modeling purposes. The detailed procedure is outlined below:

$$\mathrm{d}TP_t = dS_t + \kappa_t(S_t - T\mathrm{P})dt + \sigma_t dB_t^1 \tag{9}$$

$$\mathrm{S_t} = a_1 + b_1 t + \alpha\sin(\omega t + \varphi) \tag{10}$$

In the formula, TP_t represents the daily rainfall climate index, S_t denotes the long-term trend and seasonal variation, κ_t signifies the mean reversion rate, and σ_t indicates the rainfall fluctuation. The term dS_t ensures that TP_t reverts to S_t over time. B_t^1 represents standard Brownian motion. Additionally, ω is defined as $2\pi/365$, and φ serves as the phase shift parameter, primarily adjusting the initial position of the daily climate index.

For S_t, its parameters are estimated using the least squares method. After simplification, Equation (9) transforms into Equation (11). Additionally, under the equivalent martingale measure Q, the market price of risk λ_t is incorporated into this model [17]. This incorporated market price can be treated as a piecewise continuous function. Consequently, Equation (10) is reformulated as Equation (12).

$$\mathrm{d}TP_t = dS_t + [\kappa_t(S_t - TP_t) - \lambda_t\sigma_t]dt + \sigma_t d\widetilde{B}_t^1 \tag{11}$$

$$\mathrm{S_t} = a_1 + b_1 t + \mathrm{c_1}\sin\omega t + \mathrm{d_1}\cos\varphi t \tag{12}$$

Among these, $c_1 = \alpha\cos\varphi$ and $d_1 = \alpha\sin\varphi$. $\widetilde{B}_t^1$ represent the standard Brownian motions under the equivalent martingale measure Q.

Second, given that σ_t may exhibit seasonality and periodicity, it is also represented by the Ornstein-Uhlenbeck (O-U) model as follows:

$$\mathrm{d}\sigma_t = dY_t + \theta_t(Y_t - \sigma_t) + X_t dB_t^2 \tag{13}$$

$$\mathrm{Y_t} = \mathrm{a_2} + \beta\sin(\omega t + \varphi) \tag{14}$$

Among these components, X_t denotes climate fluctuations, B_t^2 represents the standard Wiener process, and Y_t captures the long-term trend along with seasonal variations. The long-term trend is not a static value but rather a time-varying function. The parameters are estimated using the least squares method, leading to the following simplified equation [16]:

$$\mathrm{Y_t} = \mathrm{a_2} + \mathrm{c_2}\sin\omega t + d_2\cos\omega t \tag{15}$$

Among them, $c_2 = \beta \cos\varphi$, and $d_2 = \beta \sin\varphi$.

Furthermore, with regard to the fluctuations in the climate index, while the year-on-year changes are relatively insignificant, the month-on-month variations are notably pronounced. Consequently, σ_t should be considered as a piecewise continuous function [17]. The formula for the monthly volatility of rainfall is expressed as:

$$\sigma_{y,\mathrm{m}} = \sqrt{\frac{1}{N_m - 1}\sum_{i=1}^{N_m}(T\mathrm{P}_i - \overline{T\mathrm{P}}_{y,m})^2} \tag{16}$$

$$\overline{\mathrm{TP}}_{\mathrm{y,m}} = \frac{1}{N_m}\sum_{i=1}^{N_m} T\mathrm{P}_i \tag{17}$$

Among these, the daily climate index is denoted by TP_i. $\overline{\mathrm{TP}}_{\mathrm{y,m}}$ represents the average climate index. $\sigma_{y,m}$ explains the standard deviation of the climate index in the m-th month of year y. N_m shows the total number of days in that month. The estimations of X_t and θ_t employ the quadratic variation method and the martingale estimation method proposed by Alaton et al. (2002), with the corresponding expressions given as follows [17]:

$$\mathrm{X}_{\mathrm{m}}^2 = \frac{1}{\mathrm{N_m}} = \sum_{\mathrm{i=1}}^{\mathrm{N_m\text{-}1}}(\sigma_{m,i+1} - \sigma_{m,i})^2 \tag{18}$$

$$\theta_{\mathrm{m}} = \text{-}\ln\left(\frac{\sum_{i=0}^{N_m}\frac{(\mathrm{Y_{t\text{-}1}} - \sigma_{\mathrm{t\text{-}1}})}{\mathrm{X}_{\mathrm{m}}^2}(\sigma_t - \mathrm{Y_t})}{\sum_{\mathrm{i=0}}^{\mathrm{N_m}}\frac{(\mathrm{Y_{t\text{-}1}} - \sigma_{\mathrm{t\text{-}1}})}{\mathrm{X}_{\mathrm{m}}^2}(\sigma_{t-1} - \mathrm{Y_{t\text{-}1}})}\right) \tag{19}$$

Among these, X_m^2, $\sigma_{m,t}$, and θ_m respectively denote the volatility, standard deviation of climatic conditions, and the mean reversion rate of climatic fluctuations in the m-th month. Additionally, κ_t is a piecewise continuous function that adjusts according to temporal variations. The estimation methodology for κ_t parallels that of θ_t. Based on the aforementioned estimation outcomes, by refining Equation (11), we can derive a forecast for λ_t, with the corresponding expression being:

$$\lambda_{\mathrm{t}} = \frac{\Delta \mathrm{S_t} + \kappa_{\mathrm{t}}(\mathrm{S_t} - \mathrm{T_t}) - \Delta \mathrm{T}_t}{\sigma_{\mathrm{t}}} \tag{20}$$

The Option Pricing Model

Regarding the current situation, compared to the domestic market, the international market offers a greater variety and volume of climate index derivatives. For instance, the Chicago Mercantile Exchange primarily trades climate futures, with trading periods typically defined on a monthly or quarterly basis. Commonly used climate indices include the Cumulative Average Temperature (CAT), Heating Degree Days (HDD), and Cooling Degree Days (CDD). CAT is predominantly utilized in regions where climate variability is minimal. Meanwhile, HDD and CDD are comprehensively employed based on existing climate change characteristics to achieve reasonable pricing of derivatives. The calculation formulas are as follows [16]:

$$\mathrm{H_i} = \max(0, T\mathrm{P}_\delta - TP_i) \tag{21}$$

$$\mathrm{C_i} = \max(0, T\mathrm{P}_i - TP_\delta) \tag{22}$$

Among these, H_i denotes the HDD, C_i denotes the CDD. TP_δ represents the benchmark climate index, while TP_i represents the climate index for the i-th day. HDDs signify the cumulative heating index, which is calculated as the summation of H_i values. Similarly, CDDs signify the cumulative cooling index, which is calculated as the summation of C_i values.

From the perspective of purchasing HDD call options, let V_t^h denote the contract price of the option at time t. Under identical conditions, the contract price of the HDD European put option at time t is denoted as P_t^h. The respective calculation formulas are presented as follows [18]:

$$\mathrm{V_t^h} = e^{-r_f(T_1 - t)} N_{p1} E\{\max(\mathrm{H}(0,t) + \mathrm{H}(t,\mathrm{T_1}) - K_1, 0)\} \tag{23}$$

$$\mathrm{P_t^h} = e^{-r_f(T_1 - t)} N_{p1} E\{\max(\mathrm{K_1} - \mathrm{H}(0,t), -\mathrm{H}(t,\mathrm{T_1}), 0)\} \tag{24}$$

In the formula, r_f denotes the risk-free interest rate. T and t represent the contract's expiration date and the current time, respectively. N_{p1} and K_1 signify the nominal value and strike price of the unit climate index, respectively. The HDDs during the period from t_1 to t_2 are denoted by $H(t_1, t_2)$, with the actual value represented as H(0, t). The Monte Carlo simulation predicted value for the corresponding period is indicated by H(t+1, T).

Similarly, when considering the purchase of a CDD call option, the contract price of the call option at time t is denoted as V_t^c. Under identical conditions, the contract price of the CDD European put option at time t is represented as P_t^c. The respective calculation formulas are presented below:

$$\mathrm{V_t^c} = e^{-r_f(T_2 - t)} N_{\mathrm{p_2}} E\{\max(C(0,t) + C(t,\mathrm{T_2}) - K_2, 0)\} \tag{25}$$

$$\mathrm{P_t^c} = e^{-r_f(T_2 - t)} N_{\mathrm{p2}} E\{\max(\mathrm{K_2} - C(0,t), -C(t,\mathrm{T_2}), 0)\} \tag{26}$$

In the formula, N_{p2} represents the nominal value of the unit climate index, K_2 denotes the strike price, $C(t_1,t_2)$ signifies the CDDs from time t_1 to t_2, C(0,t) indicates the actual observed value, and C(t,T) represents the forecasted value.

Research Area

The Yangtze River, as the main artery of China's ecology, plays a crucial role in conserving water sources, regulating the climate, purifying the air, and nourishing the ecosystem [19]. However, extreme climate events such as rainstorms and floods often cause damage to the ecological environment, triggering a series of problems such as soil erosion, reduction in biodiversity, and degradation of ecosystem functions. Studying the weather derivatives of the Yangtze River Economic Belt will help alleviate these extreme climate risks, effectively protect the ecological environment, and thereby promote the green and sustainable development of the region [20].

Data Source

The theory of climate system dynamics underscores the critical role of rainfall in the formation of extreme climates. Daily rainfall data have been selected as the fundamental dataset for this analysis. This data originates from the National Oceanic and Atmospheric Administration (NOAA) of the United States, providing ground meteorological information pertinent to our country [21]. For this study, all provinces within the Yangtze River Economic Belt have been included, with the temporal coverage spanning daily precipitation data from January 1, 2004, to December 31, 2023. Notably, the obtained precipitation data are recorded in inches and must be converted to millimeters for subsequent analysis.

Table 1. Results of the Unit Root Test.

Variables	ADF Statistic	P
T_{SC}	-6.536	0.000
T_{HB}	-10.006	0.000
T_{AH}	-14.004	0.000
T_{YN}	-6.047	0.000
T_{HN}	-10.185	0.000
T_{JS}	-13.811	0.000
T_{JX}	-13.811	0.000
T_{ZJ}	-11.523	0.000
T_{GZ}	-8.134	0.000
T_{SH}	-34.143	0.000
T_{CQ}	-9.459	0.000

Stationarity Test

Both SARIMA and ARIMA models fall under the umbrella of time series analysis. Before constructing these models, it is crucial to ensure the stationarity of the time series, making stationarity testing the primary task. The Autoregressive Integrated Moving Average (ARIMA) test is a more rigorous statistical method commonly used to verify time series stationarity. The validation results using the ADF test are shown in Table 1 below. The results indicate that all variables are stationary at the 1% significance level. These results confirm that the data meet the stationarity requirements, rendering them suitable for subsequent model construction and analytical work.

Results and Discussion

Construction and Prediction of Climate Models

Construction and Prediction of SARIMA Model

Model Construction

The establishment of the SARIMA model first requires the determination of the selection of p and q in the ARIMA(p, q) model. Usually, the values of p and q are 1, 2, or 3. Specifically, it is necessary to combine the information criteria of different combinations, compare the significance of the coefficients, and select the appropriate model using the Akaike Information Criterion [22].

After comparing the AIC values presented in Table 2, it is evident that for Sichuan's rainfall data, the ARIMA(1,1) model yields the lowest AIC value. Consequently, both p and q are set to 1. Similarly, for other provinces, the models are selected based on the minimum AIC criterion. Specifically, Anhui, Jiangsu, and Zhejiang adopt the ARIMA(1,1) model to describe rainfall patterns. Hubei, Jiangxi, Guizhou, and Shanghai utilize the ARIMA(0,1) model, Hunan employs the ARIMA(1,2) model, while Yunnan and Chongqing opt for the ARIMA(2,2) model.

Following the model trials, the SARIMA(1,0,1)$(1,1,1)_{12}$ model with a 12-month seasonal period was ultimately selected for the rainfall models of Sichuan, Anhui, Jiangsu, and Zhejiang. For Hubei, Jiangxi, Guizhou, and Shanghai, the SARIMA(0,0,1)$(1,1,1)_{12}$ model with a 12-month seasonal period was chosen. The SARIMA(1,0,2)$(1,1,1)_{12}$ model with a 12-month seasonal period was adopted for Hunan, while Yunnan and Chongqing utilized the SARIMA(2,0,2)$(1,1,1)_{12}$ model with a 12-month seasonal period. The autocorrelation function (ACF) plots of residuals across provinces are presented in Fig. 1. The ACF diagrams show that none of the residual coefficients exceed the upper boundary of the 95% confidence interval, indicating low autocorrelation. Based on this analysis, we obtained

the parameter coefficients for each model, as detailed in Table 3. As shown in Table 3, most parameters demonstrate statistical significance, further validating the appropriateness of the selected models.

Model Prediction

Based on the aforementioned model, the rainfall data for the Yangtze River Economic Belt from January 2024 to December 2026 were forecasted. As illustrated in Fig. 2, the predicted values exhibit

Table 2. The AIC values of the model.

AIC			q		
			0	1	2
p	T_{SC}	0	1490.182	1381.568	1376.368
		1	1436.960	1374.727	1376.055
		2	1432.301	1375.012	1376.143
	T_{HB}	0	1749.954	1602.886	1604.440
		1	1671.135	1604.334	1606.886
		2	1657.419	1603.055	1605.000
	T_{AH}	0	1661.916	1544.988	1540.963
		1	1614.584	1540.616	1543.494
		2	1591.610	1542.472	1543.754
	T_{YN}	0	1470.662	1404.856	1382.875
		1	1445.470	1380.676	1382.650
		2	1437.177	1382.640	1372.850
	T_{HN}	0	1810.179	1672.650	1672.648
		1	1769.603	1673.035	1672.617
		2	1733.839	1672.849	1674.842
	T_{JS}	0	1707.764	1579.916	1578.671
		1	1651.107	1578.298	1579.724
		2	1632.576	1579.654	1581.642
	T_{JX}	0	1942.779	1791.000	1792.798
		1	1883.949	1792.806	1794.435
		2	1852.022	1794.720	1796.355
	T_{ZJ}	0	1878.747	1717.361	1719.334
		1	1814.559	1719.335	1721.361
		2	1780.822	1721.187	1723.132
	T_{GZ}	0	1649.502	1553.536	1544.094
		1	1612.091	1543.028	1544.996
		2	1600.667	1544.981	1545.929
	T_{SH}	0	1876.446	1734.028	1734.947
		1	1822.152	1734.990	1736.817
		2	1797.541	1736.866	1738.563
	T_{CQ}	0	1594.908	1595.922	1590.927
		1	1595.636	1596.588	1592.033
		2	1592.767	1594.675	1584.098

a strong fit with the original data within the confidence interval. Furthermore, the Root Mean Square Errors (RMSEs) of the SARIMA(1,0,1)(1,1,1)$_{12}$ model applied in Sichuan, Anhui, Jiangsu, and Zhejiang were 3.673, 5.566, 5.22, and 8.352, respectively. The RMSEs for the SARIMA(0,0,1)(1,1,1)$_{12}$ model utilized in Hubei, Jiangxi, Guizhou, and Shanghai were 6.585, 9.523, 3.513, and 8.79, respectively. For Hunan, the RMSE of the SARIMA(1,0,2)(1,1,1)$_{12}$ model was 7.403, while the RMSEs for the SARIMA(2,0,2)(1,1,1)$_{12}$ model in Yunnan and Chongqing were 6.566 and 6.05, respectively. Given the low RMSE values across all provinces,

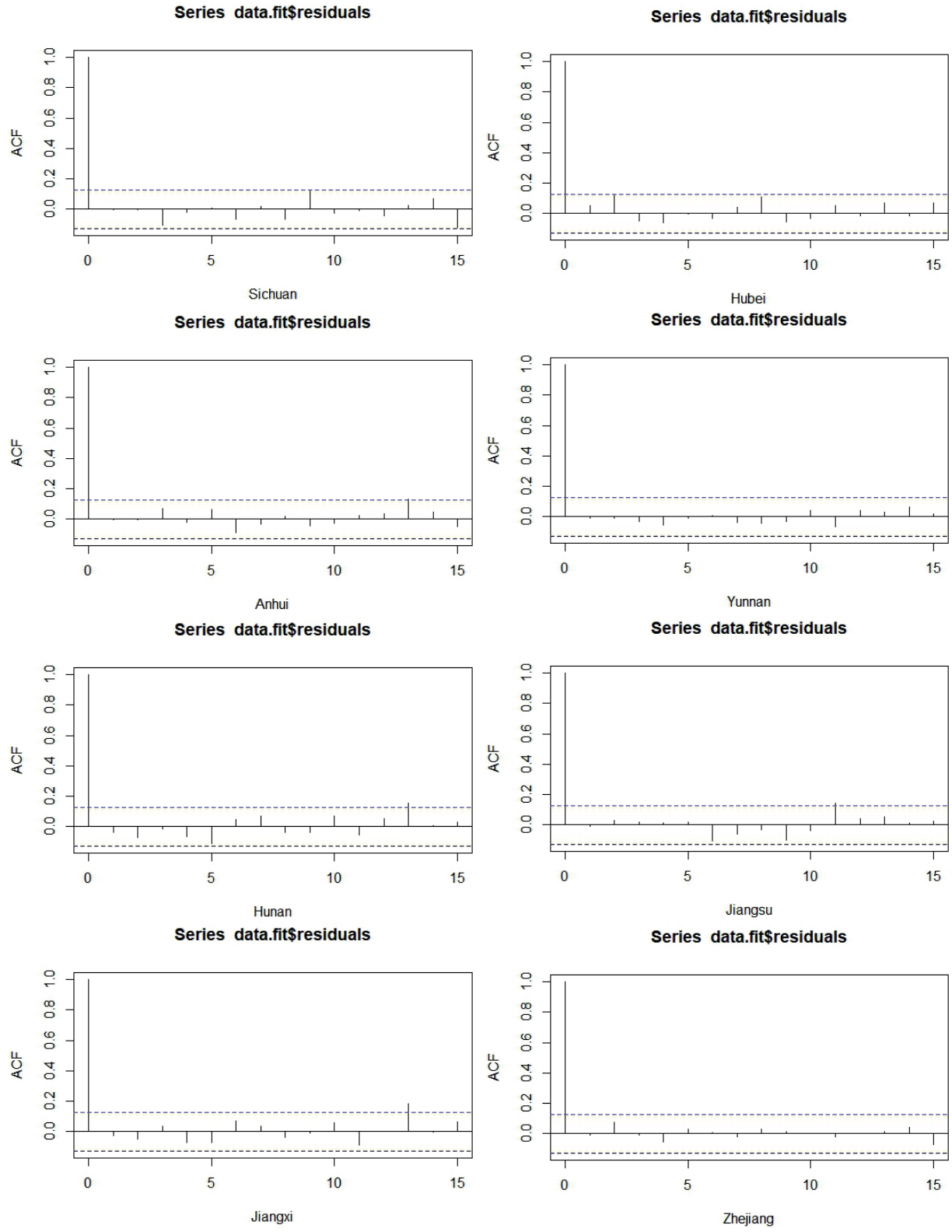

Fig. 1. ACF Chart.

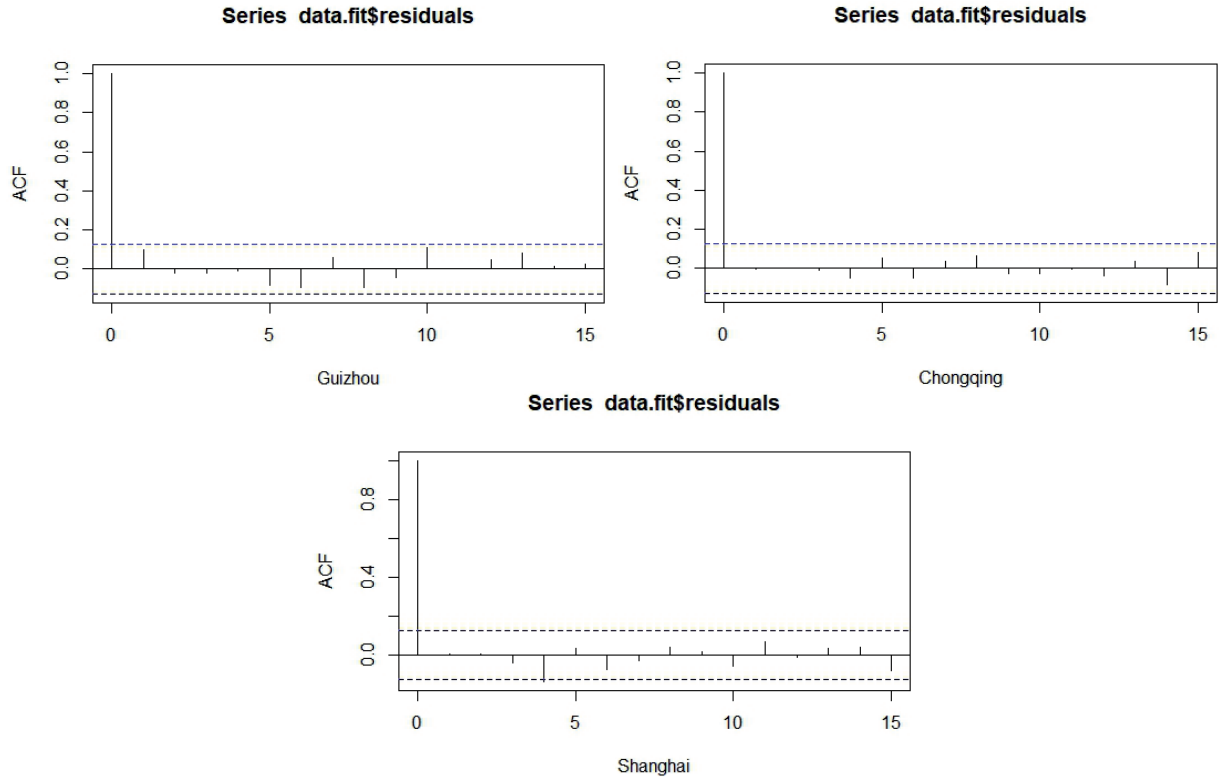

it can be concluded that the prediction error is minimal, indicating that this model is suitable for forecasting rainfall in each region.

Construction and Prediction of the OU Model

Model Construction

The OU model was used to fit the rainfall index (P_t) and rainfall fluctuation (σ_t), and the estimated results of its fitting parameters are respectively presented in Tables 4 and 5. Given that the P-values of S_t and Y_t are mostly significant, the fitting effect of the OU model is good. In addition, after discretizing Formula (13) and without considering the disturbance term, the fluctuation σ_m of precipitation for 12 months was calculated.

By conducting an autocorrelation function (ACF) test on the σ_t residuals, we can assess the model's fitting performance. The ACF of the σ_t residuals is illustrated in Fig. 3. Examination of Fig. 3 indicates that the lagged values are minimal, suggesting insignificant autocorrelation. Based on the analysis of these graphical representations, it can be concluded that the OU model exhibits satisfactory fitting performance.

Based on the foregoing analysis, it is evident that the OU model exhibits a highly satisfactory fitting effect on the rainfall index, thereby yielding the parameter estimates κ_t and λ_t. Through these parameters, significant variations in the rainfall characteristics across different provinces become apparent. To elucidate this observation, the data from Sichuan Province were selected as a case study. For detailed results, please refer to Table 6. As shown in Table 6, κ_t and λ_t in Sichuan Province exhibit contrasting trends. Similarly, when examining the data of other provinces, analogous findings are observed. This suggests that during periods of substantial rainfall fluctuation, the rate at which rainfall returns to its mean is relatively slow, and under the equivalent martingale measure, the market price of risk is correspondingly higher.

Model Prediction

Based on the histogram and QQ plot of the σ_t residuals, it is evident that the OU model exhibits a satisfactory fitting performance. Consequently, the OU model was utilized to forecast daily rainfall in 2023. It offers robust data support for the pricing strategy of future weather derivatives, thereby presenting new opportunities for mitigating climate risks.

Option Contract Design

Model Comparison

To ensure the optimal performance of multiple models in fitting climate data, this study selected the 2023 climate data from the Yangtze River Economic Belt. By applying the SARIMA and OU models in conjunction with Monte Carlo (MC) simulation technology, we predicted and analyzed HDDs and CDDs. The performance of these two models in climate prediction was evaluated by comparing their predicted values with actual observed values and calculating

Table 3. The parameter regression results of the SARIMA Model.

	T_{SC}	T_{HB}	T_{AH}	T_{YN}	T_{HN}	T_{JS}	T_{JX}	T_{ZJ}	T_{GZ}	T_{SH}	T_{CQ}
AIC	1281.03	1546.62	1489.3	1294.75	1619.95	1183.91	1726.24	1668.44	1484.64	1684.34	1531.02
ar1	-0.0012		0.122***	-0.570**	-0.533*	-0.021		-0.053			-0.002
ar2				-0.017							0.087
ma1	-1.000***	-1.000***	-1.000***	-0.333	-0.383	-0.955***	-0.970***	-0.984***	-0.959***	-1.000***	-0.992*
ma2				-0.666***	-0.616***						-0.007***
sar1	-0.058	-0.018	0.029	-0.097	0.069	-0.023	-0.072	0.143*	0.245***	-0.099	0.035
sma1	-0.840***	-0.881***	-1.000***	-0.999***	-1.000***	-0.883***	-1.000***	-1.000***	-1.000***	-0.922***	-0.999***

Table 4. Estimation results of S_t.

Provinces	Parameter	Estimated value	Standard error	t	P
Sichuan Province	a_1	-0.467	0.044	-10.57	0.000
	b_1	0.001	10.000	1.26	0.205
	c_1	-0.602	0.031	-19.25	0.000
	d_1	-1.840	0.031	-58.85	0.000
Hubei Province	a_1	-1.104	0.070	-15.78	0.000
	b_1	0.001	0.001	0.90	0.370
	c_1	-0.064	0.049	1.31	0.190
	d_1	-1.377	0.049	-27.85	0.000
Anhui Province	a_1	-0.707	0.068	-10.29	0.000
	b_1	-0.001	0.001	-2.38	0.017
	c_1	-0.203	0.048	-4.18	0.001
	d_1	-0.856	0.048	-17.62	0.000
Yunnan Province	a_1	-0.489	0.042	-11.54	0.000
	b_1	0.001	0.001	1.92	0.054
	c_1	-0.689	0.030	-22.95	0.000
	d_1	-2.195	0.029	-73.21	0.000
Hunan Province	a_1	-0.539	0.064	-8.39	0.000
	b_1	0.001	0.001	2.01	0.044
	c_1	0.429	0.045	9.45	0.000
	d_1	-1.049	0.045	-23.09	0.000
Jiangsu Province	a_1	-0.851	0.068	-12.50	0.000
	b_1	-0.001	0.001	-1.49	0.136
	c_1	-0.371	0.048	-7.71	0.000
	d_1	-0.740	0.048	-15.38	0.000
Jiangxi Province	a_1	-0.395	0.065	-6.04	0.000
	b_1	0.001	0.001	1.38	0.168
	c_1	0.533	0.046	11.51	0.000
	d_1	-0.948	0.046	-20.51	0.000
Zhejiang Province	a_1	-0.319	0.064	-4.98	0.000
	b_1	-0.001	0.001	-0.25	0.803
	c_1	0.029	0.045	0.64	0.522
	d_1	-0.822	0.045	-18.13	0.000
Guizhou Province	a_1	-0.528	0.050	-10.42	0.000
	b_1	0.001	0.001	4.22	0.000
	c_1	0.003	0.035	0.925	0.000
	d_1	-1.296	0.035	-36.16	0.000
Shanghai City	a_1	-0.497	0.056	-8.77	0.000
	b_1	-0.001	0.001	-0.57	0.570
	c_1	-0.070	0.040	-1.76	0.078
	d_1	-0.125	0.040	-3.13	0.001
Chongqing City	a_1	-0.834	0.060	-13.71	0.000
	b_1	0.001	0.001	2.20	0.027
	c_1	-0.261	0.043	-6.07	0.000
	d_1	-1.351	0.043	-31.40	0.000

Table 5. Estimation results of Y_t.

Provinces	Parameter	Estimated value	Standard error	t	P
Sichuan Province	a_2	-0.419	0.022	-18.95	0.000
	c_2	-0.604	0.031	-19.32	0.000
	d_2	-1.840	0.031	-58.85	0.000
Hubei Province	a_2	-1.050	0.034	-30.02	0.000
	c_2	-0.066	0.049	-1.34	0.178
	d_2	-1.377	0.049	-27.85	0.000
Anhui Province	a_2	-0.849	0.034	-24.70	0.000
	c_2	-0.199	0.048	-4.09	0.000
	d_2	-0.856	0.048	-17.61	0.000
Yunnan Province	a_2	-0.419	0.021	-19.76	0.000
	c_2	-0.691	0.030	-23.04	0.000
	d_2	-2.195	0.029	-73.20	0.000
Hunan Province	a_2	-0.427	0.032	-13.31	0.000
	c_2	0.426	0.045	9.38	0.001
	d_2	-1.048	0.045	-23.09	0.000
Jiangsu Province	a_2	-0.939	0.034	-27.59	0.000
	c_2	-0.368	0.048	-7.65	0.000
	d_2	-0.740	0.048	-15.38	0.000
Jiangxi Province	a_2	-0.317	0.032	-9.71	0.000
	c_2	0.530	0.046	11.46	0.000
	d_2	-0.948	0.046	-20.51	0.000
Zhejiang Province	a_2	-0.333	0.032	-10.40	0.000
	c_2	0.029	0.045	0.65	0.000
	d_2	-0.822	0.045	-18.13	0.000
Guizhou Province	a_2	-0.343	0.025	-13.53	0.000
	c_2	-0.002	0.035	-0.07	0.000
	d_2	-1.295	0.035	-36.11	0.000
Shanghai City	a_2	-0.525	0.028	-18.54	0.000
	c_2	-0.069	0.040	-1.74	0.000
	d_2	-0.125	0.040	-3.13	0.001
Chongqing City	a_2	-0.718	0.030	-23.61	0.000
	c_2	-0.265	0.043	-6.16	0.000
	d_2	-1.351	0.043	-31.39	0.000

the corresponding error metrics. For the calculation of the cumulative index, we adopted the practice of the Chicago Mercantile Exchange, using the average rainfall in the Yangtze River Economic Belt as the benchmark. In simulating rainfall changes, the SARIMA model (referred to as M1) was utilized for fitting, while the OU model (referred to as M2) was employed to describe the fluctuation characteristics of rainfall with a fixed mean reversion rate. Based on the M2 model, the mean reversion speed of rainfall fluctuation was modified to become a time-varying function, thereby addressing the issue where the residual term failed to pass the normality test. The enhanced model was designated as M3. In conjunction with MC simulation techniques, the three models were further evaluated through 10,000 simulations to derive the rainfall index. Relative error was utilized to assess the accuracy of these models, with detailed results presented in Table 7. According to the simulation outcomes in Table 7, it is evident that the M1 model exhibits lower relative errors in predicting HDDs and CDDs for the Yangtze River Economic Belt. Although the M3 model demonstrates smaller relative errors in some instances, the difference between it and the M1 model is not statistically significant. Consequently, the M1 model provides a more stable and accurate fit for the Yangtze River Economic Belt compared to the other two models. Based on this analysis, we decided to adopt the SARIMA model's prediction results for pricing options in the Yangtze River Economic Belt.

Option Pricing

Following a comprehensive comparative analysis of the aforementioned models, it is evident that the SARIMA model exhibits a significant advantage in forecasting rainfall within the Yangtze River Economic Belt. Consequently, the daily rainfall data for 11 provinces in the Yangtze River Economic Belt in 2024, as predicted by the SARIMA model, will be utilized. Additionally, the European pricing method will be employed to conduct an in-depth study on rainfall option pricing [23]. Prior to initiating the option pricing process, it is imperative to establish its fundamental elements. First, the time element pertinent to the option must be defined. Considering the substantial role of weather derivatives in mitigating extreme climate risks in agriculture and the Yangtze River Economic Belt being a major rice-producing region, the contract's validity period should be set from early May to late July, aligning with the entire growth cycle of rice and accommodating widespread contract demand [24]. Second, the nominal value must be determined. Initially, the CME established the nominal value of the rainfall index futures contract at $100 per index unit, which was excessively high for medium and small investors, thereby hindering their market participation. To attract these investors, the contract specifications were adjusted downward in 2004. Drawing upon the adjustment experience of rainfall index futures contract specifications, to facilitate farmers' participation in and transfer of climate risks, the specification for climate index futures contracts in China can be set at 10 yuan per index point. Additionally, regarding the selection of the risk-free interest rate, the Shanghai Interbank Offered Rate (SHIBOR) is chosen as the benchmark.

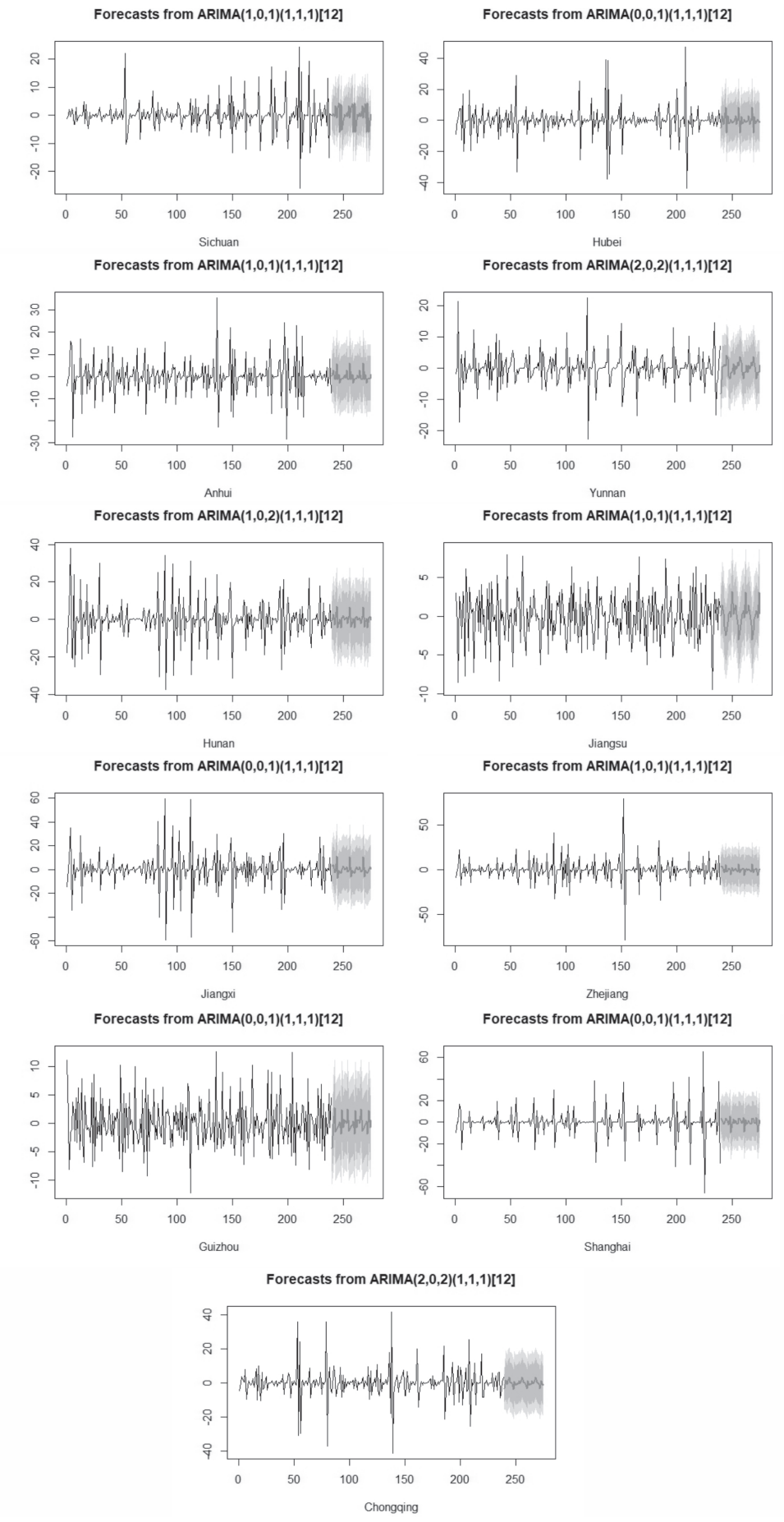

Fig. 2. Prediction fitting diagram.

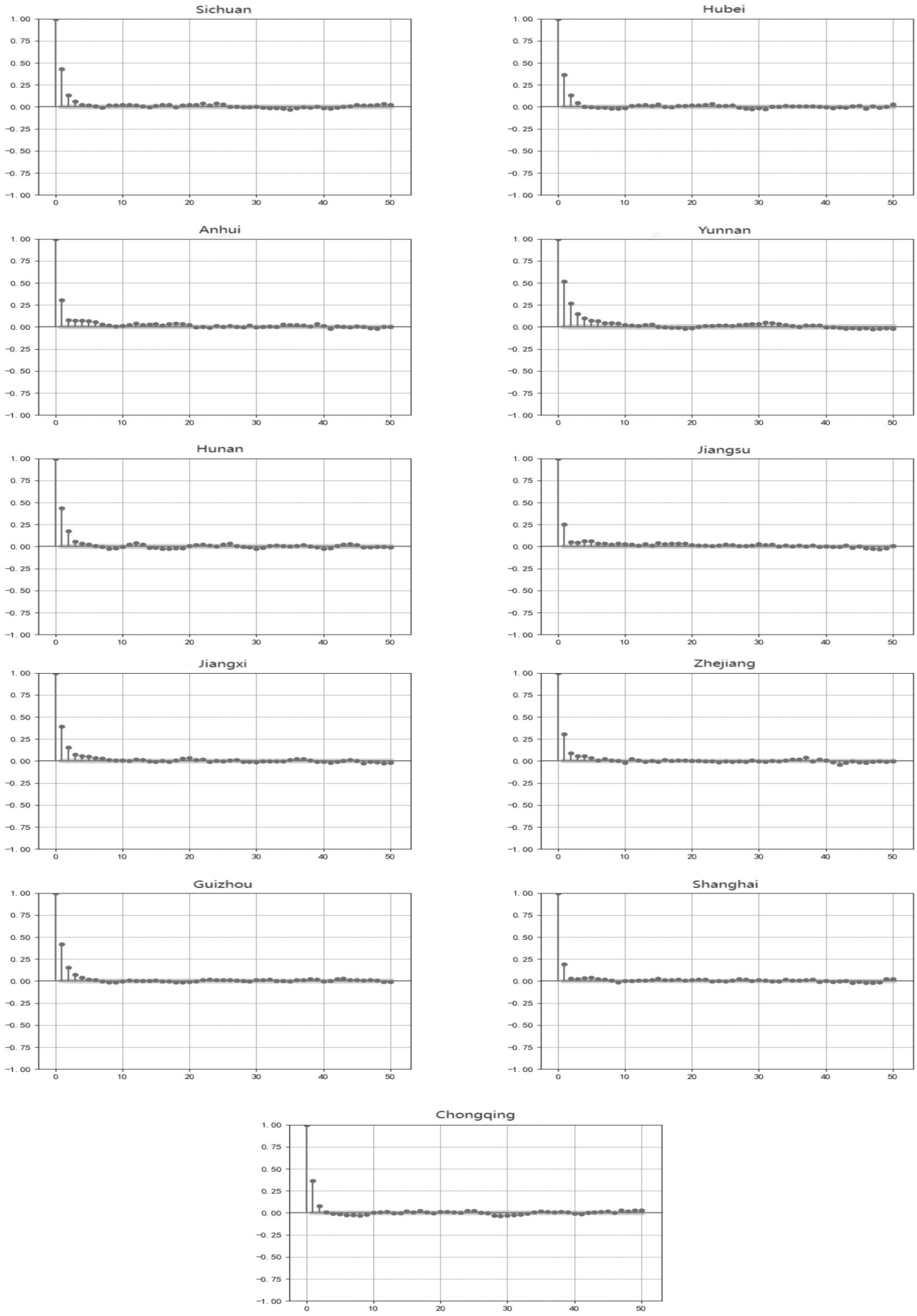

Fig. 3. ACF diagram of σ_t.

Table 6. Parameter estimation results.

Month	σ_t	θ_t	X_t	κ_t	λ_t
1	2.397	0.479	0.096	0.097	0.437
2	2.277	0.459	0.095	0.098	0.419
3	2.206	0.453	0.088	0.106	0.416
4	1.889	0.445	0.077	0.087	0.413
5	1.690	0.402	0.067	0.110	0.376
6	1.283	0.387	0.052	0.112	0.368
7	1.313	0.388	0.052	0.087	0.368
8	1.482	0.480	0.059	0.107	0.453
9	1.602	0.546	0.065	0.090	0.512
10	1.607	0.573	0.064	0.100	0.538
11	2.051	0.532	0.083	0.083	0.491
12	2.327	0.516	0.093	0.105	0.472

With the SHIBOR on May 20, 2024, being 3.45%, the risk-free interest rate is accordingly set at 3.45% [25]. Furthermore, concerning the determination of the exercise price, taking into account farmers' risk tolerance and market acceptance, the exercise price should closely reflect the actual cost of climate risks to ensure effective risk management through option contracts. According to relevant literature [26], an exercise price of 300 is selected. Given that agricultural output is significantly influenced by changes in rainfall, particularly heavy rain, which may reduce crop yields and potentially cause losses to farmers, this paper will use call options as a case study to illustrate the principles of option pricing. For detailed information, please refer to Table 8.

Table 8. European call option contracts.

The underlying index	CDDs
Exercise price	300
Contract period	2024.5.1-2024.7.31
Contract value	1CDDs = 10CNY
Location	The Yangtze River Economic Belt
Payment method	Cash

Note: CNY stands for Chinese Yuan.

In conjunction with the aforementioned fundamental parameter configurations and utilizing the option pricing model, we can calculate the price of call options for the Yangtze River Economic Belt, as detailed in Table 9. Taking Sichuan's call option as an example,

Table 7. Comparative analysis of prediction outcomes.

Provinces	M1		M2		M3	
	HDDs	CDDs	HDDs	CDDs	HDDs	CDDs
Sichuan Province	230 (0.91)	451.07 (0.33)	231.59 (0.22)	449.04 (0.33)	232.56 (0.19)	435.70 (0.29)
Hubei Province	227.92 (0.25)	294.33 (0.45)	225.10 (0.23)	465.27 (1.29)	225.50 (0.23)	387.06 (0.90)
Anhui Province	200.19 (0.10)	268.16 (0.28)	235.84 (0.30)	309.24 (0.48)	219.81 (0.21)	308.37 (0.48)
Yunnan Province	239.37 (2.50)	380.21 (0.22)	239.62 (2.4)	387.5 (0.23)	241.24 (1.74)	380.05 (0.21)
Hunan Province	358.40 (0.31)	369.84 (0.36)	389.94 (0.43)	402.51 (0.48)	387.44 (0.42)	389.35 (0.43)
Jiangsu Province	199.84 (0.05)	276.55 (0.27)	228.50 (0.2)	336.04 (0.54)	207.71 (0.09)	321.72 (0.48)
Jiangxi Province	318.54 (0.02)	488.65 (0.31)	387.71 (0.46)	519.41 (0.40)	360.77 (0.36)	485.09 (0.30)
Zhejiang Province	282.51 (0.19)	537.52 (0.51)	386.29 (0.64)	994.58 (1.79)	330.00 (0.40)	702.54 (0.97)
Guizhou Province	242.76 (2.00)	316.57 (0.16)	259.52 (4.77)	529.69 (0.95)	246.32 (0.56)	380.91 (0.40)
Shanghai City	231.68 (0.15)	409.61 (0.47)	342.1 (0.64)	649.32 (1.34)	279.75 (0.38)	419.64 (0.51)
Chongqing City	194.26 (0.07)	299.93 (0.39)	168.69 (0.06)	336.03 (0.57)	176.83 (0.01)	302.25 (0.40)

Note: The content in brackets is the relative error.

Table 9. Climate option prices.

Provinces	M1
Sichuan Province	2984.63
Hubei Province	1430.80
Anhui Province	1171.37
Yunnan Province	2282.17
Hunan Province	2179.37
Jiangsu Province	1254.54
Jiangxi Province	3357.18
Zhejiang Province	3841.65
Guizhou Province	1651.28
Shanghai City	2573.62
Chongqing City	1486.32

Note: All the digital units are in CNY.

the contract price is 2,984.63 yuan. If the actual CDDs in May, June, July, and August 2023 are 337.40 points, exceeding the strike index by 37.4 points, growers who choose to exercise the option can receive a cash payment of 374 yuan on the first trading day of September. Therefore, purchasing this option can mitigate the impact of weather risks on asset price volatility. In the event of extreme climates, higher CDDs would further enhance risk transfer capabilities under such conditions. Additionally, based on the model's pricing results, it is observed that provinces with higher rainfall levels (such as Zhejiang, Jiangxi, and Sichuan) generally have higher option prices. Particularly during June, July, and August, precipitation exhibits significant fluctuations due to the influence of the plum rain season, typhoons, and heavy storms. This suggests that greater climate volatility and higher climate risk correlate with higher option pricing, aligning with the principles of financing cost theory.

The Application of Weather Derivatives

Weather derivatives, as an emerging financial instrument, have effectively facilitated the transfer of climate-related risks. They provide insurance companies with an innovative risk management tool, enabling them to partially mitigate the financial exposure associated with extreme weather events through the trading of weather derivatives [27]. The utilization of these instruments not only enhances the ability of market participants to manage climate risks but also fosters innovation in the financial market and diversifies financial services. Specifically, the application scenarios for both buyers and sellers in the market are as follows:

For the buyer, weather derivatives provide call options with elevated strike prices and put options with reduced strike prices. These can be utilized to mitigate the risks associated with extreme climate events, such as low rainfall and excessive rainfall, respectively. Consequently, the primary beneficiaries of these options are entities that stand to incur losses due to extreme rainfall conditions, with agricultural producers and related industries being the most significant participants [28]. Weather derivatives are designed specifically for rainfall management. Producers can assess the sensitivity of their future income to rainfall levels and purchase corresponding call or put options based on their specific needs [29].

The sellers of this option are primarily entities that stand to benefit when rainfall significantly deviates from expected levels [30]. These benefits are realized through price changes in related assets. Sellers typically hold assets whose values are influenced by rainfall patterns. By employing an opposite "option + asset" strategy, these sellers can mitigate the volatility of their earnings. Research by Georgios (2017) examined the effectiveness of weather derivatives in the energy sector [31]. The study found that the company effectively stabilized its revenue despite fluctuations in hydropower production, thus confirming the value of weather derivatives in mitigating financial risks in the energy sector.

In summary, compared to traditional methods of climate risk management, weather derivatives offer several advantages, including high flexibility, objective maturity value, fewer restrictions on participants, and lower internal costs. These instruments help mitigate the volatility of future income for trading entities and provide an effective hedge against climate risks [32]. Their application in key industries such as agriculture [33] and energy [34] effectively deals with industry-specific quantitative risks and income risks caused by adverse meteorological conditions, highlighting their practical application value. Consequently, this market attracts a broad range of participants and mitigates price risks associated with market speculation.

Conclusions

This paper addresses the underexplored area of weather derivatives within climate response strategies, focusing on the Yangtze River Economic Belt. Utilizing historical rainfall data (2004-2023) and the SARIMA model for time series analysis and forecasting, this research calculated option prices based on an option pricing model and formulated a comprehensive option contract. This work contributes valuable insights for developing weather options in China and offers a novel approach for agricultural producers and investors to mitigate abnormal rainfall risks.

However, this study has several limitations that warrant acknowledgment. Firstly, while SARIMA effectively captured historical rainfall trends at the regional scale of the Yangtze River Economic Belt, the model's performance and the generalizability of the derived option pricing to more localized areas or regions with distinct climatic characteristics remain

uncertain. Furthermore, given the multifaceted and complex nature of meteorological drivers, the SARIMA model's accuracy in predicting highly irregular or extreme rainfall fluctuations, particularly those driven by non-linear processes potentially intensified under climate change, is constrained.

Future research should prioritize addressing these limitations and exploring specific avenues. Developing and validating more sophisticated modeling approaches is crucial; exploring non-parametric methods, machine learning algorithms, or hybrid models could enhance the capture of complex non-linear relationships and extreme events, leading to improved forecasting accuracy. Concurrently, investigating the design and pricing of multi-variable weather derivatives that trigger based on combinations of factors could offer more comprehensive risk mitigation against compound climate hazards.

Acknowledgement

This work did not receive funding.

Conflict of Interest

The authors declare no conflict of interest

Data Availability Statement

The data used in this study are available from the corresponding author upon reasonable request. Efforts have been made to ensure the accuracy and completeness of the data. However, the authors do not guarantee the absolute accuracy or completeness of the data, and any use of the data should be based on the user's own judgment and verification.

References

1. ZHANG M., TAN S., LIANG J., ZHANG C., CHEN E. Predicting the impacts of urban development on urban thermal environment using machine learning algorithms in Nanjing, China. Journal of Environmental Management. **356**, 120560, **2024**.
2. HE L., CHEN J., CHENG C., YUAN J., QU B., WEI Y. Evaluation and spatio-temporal analysis of social vulnerability to flood disasters in the Yangtze River Economic Belt. Water Resources and Hydropower Engineering. **55** (3), 24, **2024**.
3. ZHANG T., QI P. Construction of Rural Financial Support System and Its Potential Risks Research - Based on the Expansion of the "Insurance + Futures" Model. Investment Research. **38** (10), 42, **2019**.
4. BRESSAN G.M., ROMAGNOLI S. Climate risks and weather derivatives: A copula-based pricing model. Journal of Financial Stability. **54**, 100877, **2021**.
5. ZAPRANIS A., ALEXANDRIDIS A. Weather derivatives pricing: Modeling the seasonal residual variance of an Ornstein–Uhlenbeck temperature process with neural networks. Neurocomputing. **73** (1), 37, **2009**.
6. NHANGUMBE C., SOUSA E. Numerical solutions of an option pricing rainfall weather derivatives model. Computers & Mathematics with Applications. **153**, 43, **2024**.
7. KUMARI S., MUTHULAKSHMI P. SARIMA Model: An Efficient Machine Learning Technique for Weather Forecasting. Procedia Computer Science. **235**, 656, **2024**.
8. ZHANG M., TAN S., ZHANG C., CHEN E. Machine learning in modelling the urban thermal field variance index and assessing the impacts of urban land expansion on seasonal thermal environment. Sustainable Cities and Society. **106**, 105345, **2024**.
9. [9] CHEN T., ZHANG L., WEN M., YUAN W., LIN W. Can the development of agricultural insurance promote the resilience of agricultural economy? The dynamic mechanisms of the digital economy development. International Review of Economics & Finance. **103**, 104386, **2025**.
10. CHIDZALO P., NGARE P.O., MUNG'ATU J.K. Pricing weather derivatives under a tri-variate stochastic model. Scientific African. **21**, e01768, **2023**.
11. BUCHHOLZ M., MUSSHOFF O. The role of weather derivatives and portfolio effects in agricultural water management. Agricultural Water Management. **146**, 34, **2014**.
12. ZHANG N., TONG L. Forecast of International Demand for Ice and Snow Tourism in Heilongjiang Province Based on SARIMA Model. Resource Development & Market. **28** (7), 660, **2012**.
13. BEI H., ZHU L., WANG W., SUN Y. Research on the Pricing of Weather Derivatives Considering the Risk Market Price. Systems Engineering Theory and Practice. **42** (12), 3265, **2022**.
14. LI Y., XIA M., LIANG L. Research on the pricing of weather derivatives based on the O-U model - Taking temperature options as an example. Forecasting. (2), 18, **2012**.
15. WANG Q., HE Z. Challenges and Countermeasures Faced by China's Tourism Industry in the Post-epidemic Period: Taking Jilin City, Jilin Province as an Example. China Soft Science. (S1), 147, **2020**.
16. ZHENG T., HAN X., TAO X., JI Y. Exploratory Research on Temperature Prediction Models of Weather Derivatives. Journal of Zhejiang University. **51** (5), 553, **2023**.
17. ALATON P., DJEHINCE B., STILLBERG D. On modeling and pricing weather derivatives. Applied Mathematical Finance. **9** (1), 1, **2002**.
18. BERHANE T., SHIBABAW A., AWGICHEW G. Pricing Weather Derivatives Index Based on Temperature: The Case of Bahir Dar, Ethiopia. Journal of Resources and Ecology. **10** (4), 415, **2019**.
19. WANG X., DAI Y., XU Y.J., LV Q., JI X., MAO B., JIA S., LIU Z., LUO C., RONG Y. Dual-quantification of the different contributions of climate change and anthropogenic activities to eutrophication of rivers and lakes in Asia's largest river basin (Yangtze River). Journal of Hazardous Materials. **496**, 139205, **2025**.
20. MA L., HUANG D., JIANG X., YANG L., ZHANG M., LIN Y. Does collaborative governance of natural disasters in urban agglomerations enhance urban resilience? Evidence from China. Environment, Development and Sustainability. **2025**.
21. GUILLEVIC P.C., PRIVETTE J.L., COUDERT B., PALECKI M.A., DEMARTY J., OTTLÉ C., AUGUSTINE

J.A. Land Surface Temperature product validation using NOAA's surface climate observation networks – Scaling methodology for the Visible Infrared Imager Radiometer Suite (VIIRS). Remote Sensing of Environment. **124**, 282, **2012**.
22. CHATURVEDI S., RAJASEKAR E., NATARAJAN S., MCCULLEN N. A comparative assessment of SARIMA, LSTM RNN and Fb Prophet models to forecast total and peak monthly energy demand for India. Energy Policy. **168**, 113097, **2022**.
23. **[23]** SAWANGTONG P., TAGHIPOUR M., NAJAFI A. An efficient computational method for solving the fractional form of the European option price PDE with transaction cost under the fractional Heston model. Engineering Analysis with Boundary Elements. **169**, 105972, **2024**.
24. YANG G., YANG X. Research on the Hedging Efficiency of Weather Derivatives on Agricultural Product Yield Fluctuation. Journal of Financial Development Research. (6), 81, **2020**.
25. ZHOU B., WANG J. Option Pricing of China Real Estate Index Based on OU Process. Management World. (4), 176, **2013**.
26. LI Y., SHI H., LI H. Research on the applicability of the time-varying O-U model in the pricing of agricultural temperature index insurance. Management Review. **32** (4), 3, **2020**.
27. MATSUMOTO T., YAMADA Y. Simultaneous hedging strategy for price and volume risks in electricity businesses using energy and weather derivatives. Energy Economics. **95**, 105101, **2021**.
28. SUN B., VAN KOOTEN G.C. Financial weather derivatives for corn production in Northern China: A comparison of pricing methods. Journal of Empirical Finance. **32**, 201, **2015**.
29. ZHOU R., LI J.S.H., PAI J. Hedging crop yield with exchange-traded weather derivatives. Agricultural Finance Review. **76** (1), 172, **2016**.
30. ŠTULEC I., PETLJAK K., NALETINA D. Weather impact on retail sales: How can weather derivatives help with adverse weather deviations? Journal of Retailing and Consumer Services. **49**, 1, **2019**.
31. KARAKATSANIS G., ROUSSIS D., MOUSTAKIS Y., GOURNARI P., PARARA I., DIMITRIADIS P., KOUTSOYIANNIS D. Energy, variability and weather finance engineering. Energy Procedia. **125**, 389, **2017**.
32. BERHANE T., SHIBABAW N., AWGICHEW G., KEBEDE T. Option pricing of weather derivatives based on a stochastic daily rainfall model with Analogue Year component. Heliyon. **6** (1), e03212, **2020**.
33. HOTT C., REGNER J. Weather extremes, agriculture and the value of weather index insurance. The Geneva Risk and Insurance Review. **48** (2), 230, **2023**.
34. HAN X., ZHANG G., XIE Y., YIN J., ZHOU H., YANG Y., BAI W. Weather index insurance for wind energy. Global Energy Interconnection. **2** (6), 541, **2019**.